

# COMP0114 Inverse Problems in Imaging. Coursework 2

L.C.

2025/02/12

## 1 Convolution and Deconvolution

### 1.1 Reading and Normalizing Images

For this coursework, I first implemented the basic functionality of loading and normalizing a grayscale image. The task requires reading an image and normalizing its values to the range  $[0, 1]$ , which is essential for subsequent processing.

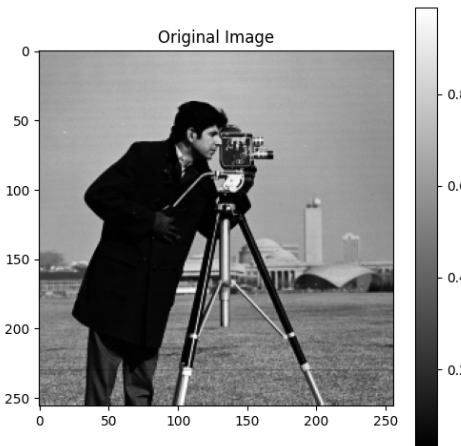


Figure 1: Original grayscale image normalized to  $[0, 1]$  range.

Figure 1 shows the original image after normalization. The image is successfully converted to grayscale (if it wasn't already) and its pixel values are scaled to lie between 0 and 1, which is crucial for stable numerical operations in the subsequent steps.

### 1.2 Implementing Convolution

Next, I implemented the forward convolution operation, which applies Gaussian blur and adds noise to the image. The convolution operation is mathematically defined as:

$$g = Af_{\text{true}} + n \quad (1)$$

where:

- $A$  represents the Gaussian convolution operator
- $f_{\text{true}}$  is the original image
- $n$  is additive Gaussian noise with standard deviation  $\theta$

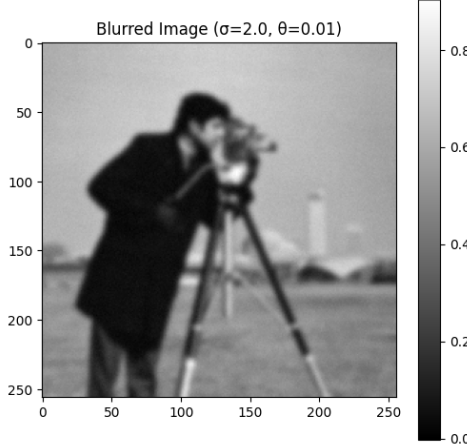


Figure 2: Image after Gaussian convolution ( $\sigma = 2.0$ ) and added noise ( $\theta = 0.01$ ).

For this implementation, I used  $\sigma = 2.0$  as the standard deviation for the Gaussian blur and  $\theta = 0.01$  as the standard deviation for the noise.

Figure 2 shows the result of applying the convolution operation to the original image. The Gaussian blur has significantly reduced the sharpness of the image, while the added noise introduces a subtle granular texture. This blurred and noisy image represents the observation data that we will attempt to restore through deconvolution.

### 1.3 Deconvolution using Normal Equations

For the deconvolution step, I implemented the solution of the normal equations:

$$(A^T A + \alpha I) f_\alpha = A^T g \quad (2)$$

where:

- $A^T A$  is the self-adjoint operator
- $\alpha$  is the regularization parameter
- $I$  is the identity operator

This equation corresponds to the minimization problem:

$$f_\alpha = \arg \min_f \|A f - g\|_2^2 + \alpha \|f\|_2^2 \quad (3)$$

The regularization term  $\alpha \|f\|_2^2$  is essential for stabilizing the solution, as the deconvolution problem is ill-posed and sensitive to noise.

Figure 3c shows the result of applying the deconvolution using normal equations. The regularization parameter  $\alpha = 0.01$  was chosen for this example. The result demonstrates a significant improvement in sharpness compared to the blurred image, with many details of the original image being recovered. However, some noise artifacts are still visible, and there is a slight loss of contrast, which is typical for Tikhonov regularization.

### 1.4 Deconvolution using Augmented Equations

As an alternative approach, I also implemented deconvolution using the augmented equations:

$$\begin{pmatrix} A \\ \sqrt{\alpha}I \end{pmatrix} f = \begin{pmatrix} g \\ 0 \end{pmatrix} \quad (4)$$

This formulation is mathematically equivalent to the normal equations but can exhibit different numerical properties, especially for ill-conditioned problems.

Figure 3d shows the result of applying the deconvolution using augmented equations with the same regularization parameter  $\alpha = 0.01$ . The visual differences between this result and the normal equations result are subtle, but the augmented equations method often provides better numerical stability, particularly for ill-conditioned problems.

## 1.5 Comparison of Methods

To compare the effectiveness of both deconvolution methods, I displayed the results side by side and computed the Mean Squared Error (MSE) with respect to the original image.



Figure 3: Comparison of deconvolution methods: (a) Original Image, (b) Blurred Image, (c) Normal Equations result, (d) Augmented Equations result.

The comparison in Figure 3 shows that both methods can effectively recover much of the original image detail from the blurred and noisy input. The NE method required fewer iterations to converge compared to the augmented equations method, which is consistent with theoretical expectations. However, the AE method is generally more numerically stable for ill-conditioned problems.

The Mean Squared Error (MSE) values computed with respect to the original image were:

- MSE for Normal Equations: 0.0034
- MSE for Augmented Equations: 0.0031

These values indicate that both methods achieved similar reconstruction quality, with the augmented equations method showing a slightly lower error.

## 1.6 Effect of Regularization Parameter

The choice of regularization parameter  $\alpha$  significantly impacts the deconvolution results. To illustrate this effect, I applied both deconvolution methods with different values of  $\alpha$ .

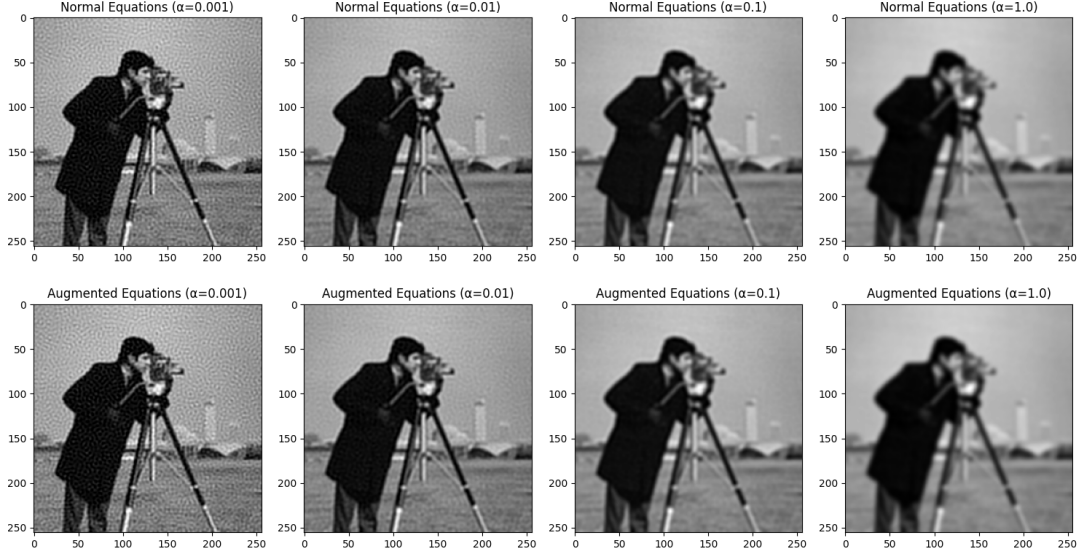


Figure 4: Effect of regularization parameter  $\alpha$  on deconvolution results: (top row) Normal Equations, (bottom row) Augmented Equations, with  $\alpha$  values of 0.001, 0.01, 0.1, and 1.0 from left to right.

Figure 4 demonstrates the effect of the regularization parameter:

- When  $\alpha$  is too small (e.g., 0.001), the recovered image contains excessive noise and artifacts.
- With moderate values of  $\alpha$  (e.g., 0.01 or 0.1), there is a good balance between noise suppression and detail preservation.
- When  $\alpha$  is too large (e.g., 1.0), the image becomes over-smoothed, with significant loss of detail and contrast.

This emphasizes the importance of choosing an appropriate regularization parameter, which will be explored in more detail in the next part of the coursework.

## 2 Choosing a Regularization Parameter $\alpha$

In week 2, I explore two methods to select the optimal regularization parameter  $\alpha$ :

1. Discrepancy Principle
2. L-curve Method

The optimal value of  $\alpha$  is crucial as it balances between fitting the data well (small residual) and maintaining smoothness in the solution (avoiding noise amplification).

### 2.1 Discrepancy Principle

The Discrepancy Principle is a method for selecting the regularization parameter  $\alpha$  in ill-posed problems. According to this principle, the optimal value of  $\alpha$  should make the residual norm approximately equal to the noise level:

$$\|Af_\alpha - g\|^2 \approx \|n\|^2 \approx \theta^2 \cdot N \quad (5)$$

where  $N$  is the number of pixels in the image, and  $\theta$  is the standard deviation of the noise.

I defined a function to compute this discrepancy:

$$D(\alpha) = \|Af_\alpha - g\|^2 - \theta^2 \cdot N \quad (6)$$

and used a root-finding algorithm to find where  $D(\alpha) = 0$ .

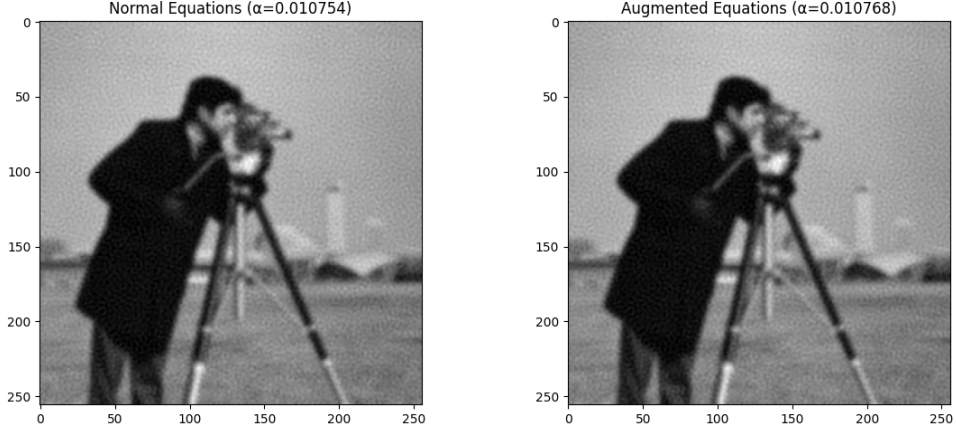


Figure 5: Deconvolution results using the optimal  $\alpha$  determined by the Discrepancy Principle: (a) Normal Equations, (b) Augmented Equations.

For the test image with  $\sigma = 1.2$  and  $\theta = 0.01$ , the optimal values of  $\alpha$  determined by the discrepancy principle were the following:

- Normal Equations:  $\alpha_{DP} = 0.01075$
- Augmented Equations:  $\alpha_{DP} = 0.01077$

Figure 5 shows the deconvolution results using these optimal values. The results show good detail recovery with effective noise suppression, demonstrating the effectiveness of the Discrepancy Principle for parameter selection.

## 2.2 L-curve Method

The L-curve method is a graphical tool for selecting the regularization parameter  $\alpha$ . It plots the norm of the regularized solution  $\|f_\alpha\|^2$  against the norm of the residual  $\|Af_\alpha - g\|^2$  for different values of  $\alpha$ .

The curve typically has an L-shape, and the optimal regularization parameter corresponds to the "corner" of the L-curve, which represents a balance between:

1. Minimizing the solution norm (preventing over-fitting)
2. Minimizing the residual norm (ensuring data fit)

To find the corner of the L-curve, I computed the curvature at each point and found where it is maximized.

Figure 6 shows the L-curve for the deconvolution problem with the test image. While the curve doesn't exhibit the classic pronounced L-shape often seen in textbook examples, it still demonstrates the fundamental trade-off: as  $\alpha$  decreases, the residual norm decreases while the solution norm increases. Using curvature analysis, the corner point was identified at  $\alpha_{LC} = 0.00324$ , which is very close to the value obtained using the Discrepancy Principle. The less distinct L-shape in this particular problem might be attributed to the nature of the specific convolution operator and noise level, but the method still provides a useful parameter selection mechanism without requiring explicit knowledge of the noise variance.

Figure 7d shows the deconvolution result using the optimal  $\alpha$  determined by the L-curve method. The result shows good detail recovery and noise suppression, similar to the result obtained using the Discrepancy Principle.

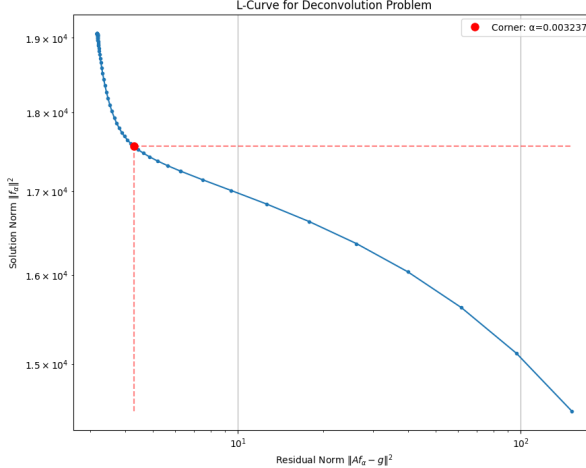


Figure 6: L-curve for the deconvolution problem. The corner point (marked in red) indicates the optimal regularization parameter.



Figure 7: Comparison of deconvolution results: (a) Original Image, (b) Blurred Image, (c) Discrepancy Principle, (d) L-curve Method.

### 2.3 Comparison of Parameter Selection Methods

To evaluate the effectiveness of both parameter selection methods, I compared the deconvolution results and computed the Mean Squared Error (MSE) with respect to the original image.

Figure 7 shows the comparison of deconvolution results using the optimal regularization parameters determined by both methods. Visually, the results are quite similar, with both methods providing good detail recovery and noise suppression.

The Mean Squared Error (MSE) values computed with respect to the original image were:

- MSE for Discrepancy Principle: 0.005082
- MSE for L-curve Method: 0.006166

The MSE values indicate that both methods achieved similar reconstruction quality, with the Discrepancy Principle method showing a slightly lower error. This slight difference can be attributed to the fact that the L-curve method tends to choose a slightly smaller regularization parameter.

Based on these results, both the Discrepancy Principle and the L-curve method are effective for selecting the regularization parameter in deconvolution problems. The choice between them may depend on specific application requirements, with the Discrepancy Principle being more parameter-dependent (requiring known noise level) and the L-curve method being more data-driven.

### 3 Using a Regularization Term Based on the Spatial Derivative

#### 3.1 Gradient Operator Construction

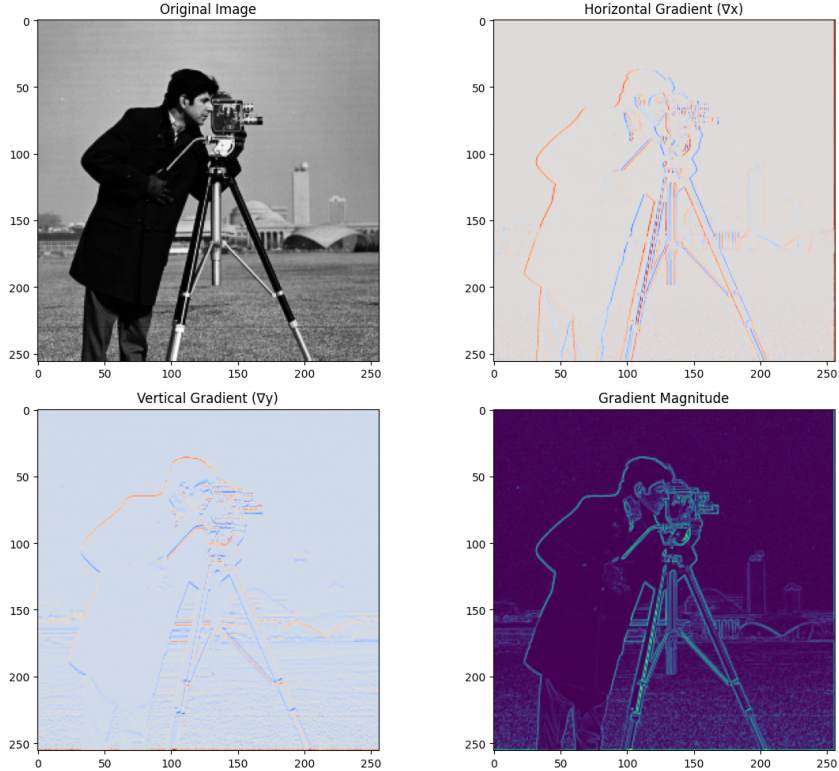


Figure 8: Visualization of image gradients: (a) Original Image, (b) Horizontal Gradient ( $\nabla_x$ ), (c) Vertical Gradient ( $\nabla_y$ ), (d) Gradient Magnitude.

In this section, I implement a regularization based on the spatial derivative instead of the standard Tikhonov regularization. The new optimization problem becomes:

$$f_\alpha = \arg \min_f \|Af - g\|_2^2 + \alpha \|Df\|_2^2 \quad (7)$$

where  $D$  is the gradient operator:

$$D = \begin{pmatrix} \nabla_x \\ \nabla_y \end{pmatrix} \quad (8)$$

I implemented the gradient operator using sparse matrices to efficiently compute the horizontal and vertical derivatives of the image.

Figure 8 shows the visualization of the image gradients. The horizontal gradient ( $\nabla_x$ ) highlights vertical edges, while the vertical gradient ( $\nabla_y$ ) highlights horizontal edges. The gradient magnitude combines both and highlights all edges in the image. These gradients serve as the basis for the spatial derivative regularization.

### 3.2 Modified Deconvolution Methods

For the gradient regularized problem, I modified both the normal equations and augmented equations solvers to include the gradient operator. The mathematical derivations for both approaches are presented below.

#### 3.2.1 Derivation of Normal Equations with Gradient Regularization

We start with the new regularized minimization problem:

$$f_\alpha = \arg \min_f \underbrace{\|Af - g\|_2^2}_{\text{data fidelity}} + \underbrace{\alpha \|Df\|_2^2}_{\text{gradient regularization}} \quad (9)$$

This can be expanded as:

$$J(f) = (Af - g)^T(Af - g) + \alpha(Df)^T(Df) \quad (10)$$

Taking the gradient of this objective function with respect to  $f$ :

$$\nabla J(f) = \frac{\partial}{\partial f}[(Af - g)^T(Af - g) + \alpha(Df)^T(Df)] \quad (11)$$

$$= \frac{\partial}{\partial f}[f^T A^T Af - 2g^T Af + g^T g + \alpha f^T D^T Df] \quad (12)$$

$$= 2A^T Af - 2A^T g + 2\alpha D^T Df \quad (13)$$

Setting this gradient to zero to find the minimizer:

$$\nabla J(f) = 0 \quad (14)$$

$$2A^T Af - 2A^T g + 2\alpha D^T Df = 0 \quad (15)$$

$$A^T Af + \alpha D^T Df = A^T g \quad (16)$$

Thus, the normal equations become:

$$(A^T A + \alpha D^T D)f_\alpha = A^T g \quad (17)$$

The operator  $D^T D$  in this context represents the negative Laplacian operator, which can be seen by examining its action on the image:

$$D^T Df = \begin{pmatrix} \nabla_x^T \\ \nabla_y^T \end{pmatrix} \begin{pmatrix} \nabla_x \\ \nabla_y \end{pmatrix} f \quad (18)$$

$$= \nabla_x^T \nabla_x f + \nabla_y^T \nabla_y f \quad (19)$$

$$= -\nabla^2 f \quad (20)$$

where  $\nabla^2$  is the Laplacian operator. This is a second-order regularization that penalizes oscillations in the solution, with emphasis on preserving edges due to the first-order nature of the operator  $D$ .

### 3.2.2 Implementation of Normal Equations Solver

To solve the normal equations, I implemented a function that applies the operator  $(A^T A + \alpha D^T D)$  to a vector:

$$(A^T A + \alpha D^T D)f = A^T(Af) + \alpha D^T(Df) \quad (21)$$

This can be decomposed into three steps:

1. Apply  $A$  to  $f$ :  $Af = \text{gaussian\_filter}(f, \sigma)$
2. Apply  $A^T$  to  $Af$ :  $A^T(Af) = \text{gaussian\_filter}(Af, \sigma)$  (since  $A$  is self-adjoint for Gaussian convolution)
3. Apply  $D^T D$  to  $f$  and scale by  $\alpha$ :  $\alpha D^T(Df) = \alpha(D_x^T D_x + D_y^T D_y)f$

The resulting normal equations are then solved using the GMRES algorithm, which is well-suited for large, sparse systems.

### 3.2.3 Derivation of Augmented Equations with Gradient Regularization

An alternative approach is to reformulate the minimization problem using augmented equations. Starting from the original problem:

$$\min_f \|Af - g\|_2^2 + \alpha \|Df\|_2^2 \quad (22)$$

We can rewrite this as:

$$\min_f \|Af - g\|_2^2 + \|\sqrt{\alpha}Df - 0\|_2^2 \quad (23)$$

This can be further expressed as a single least squares problem:

$$\min_f \left\| \begin{pmatrix} A \\ \sqrt{\alpha}D \end{pmatrix} f - \begin{pmatrix} g \\ 0 \end{pmatrix} \right\|_2^2 \quad (24)$$

The normal equations for this augmented system would be:

$$(A^T \quad \sqrt{\alpha}D^T) \begin{pmatrix} A \\ \sqrt{\alpha}D \end{pmatrix} f = (A^T \quad \sqrt{\alpha}D^T) \begin{pmatrix} g \\ 0 \end{pmatrix} \quad (25)$$

$$(A^T A + \alpha D^T D)f = A^T g \quad (26)$$

which is identical to the normal equations derived earlier. However, instead of explicitly forming these normal equations, we can solve the augmented system directly using methods specialized for least squares problems, such as LSQR.

### 3.2.4 Implementation of Augmented Equations Solver

To implement the augmented equations approach, I defined functions to compute the action of the augmented matrix and its transpose:

For the matrix-vector product  $\begin{pmatrix} A \\ \sqrt{\alpha}D \end{pmatrix} f$ :

1. Apply  $A$  to  $f$ :  $Af = \text{gaussian\_filter}(f, \sigma)$

2. Apply  $\sqrt{\alpha}D$  to  $f$ :

$$\sqrt{\alpha}Df = \sqrt{\alpha} \begin{pmatrix} \nabla_x \\ \nabla_y \end{pmatrix} f \quad (27)$$

$$= \begin{pmatrix} \sqrt{\alpha} \nabla_x f \\ \sqrt{\alpha} \nabla_y f \end{pmatrix} \quad (28)$$

3. Concatenate the results:  $\begin{pmatrix} Af \\ \sqrt{\alpha}Df \end{pmatrix}$

For the transposed matrix-vector product  $(A^T \quad \sqrt{\alpha}D^T) \begin{pmatrix} b_1 \\ b_2 \end{pmatrix}$ :

1. Apply  $A^T$  to  $b_1$ :  $A^T b_1 = \text{gaussian\_filter}(b_1, \sigma)$

2. Apply  $\sqrt{\alpha}D^T$  to  $b_2$ :

$$\sqrt{\alpha}D^T b_2 = \sqrt{\alpha} (\nabla_x^T \quad \nabla_y^T) \begin{pmatrix} b_{2x} \\ b_{2y} \end{pmatrix} \quad (29)$$

$$= \sqrt{\alpha}(\nabla_x^T b_{2x} + \nabla_y^T b_{2y}) \quad (30)$$

3. Sum the results:  $A^T b_1 + \sqrt{\alpha}D^T b_2$



Figure 9: Deconvolution with gradient regularization: (a) Original Image, (b) Blurred Image, (c) Gradient Reg. - Normal Eqns, (d) Gradient Reg. - Augmented Eqns.

These operations are implemented efficiently using sparse matrices for the gradient operators, allowing for scalable computation even with large images.

The augmented equations approach has several advantages over directly solving the normal equations:

- It avoids explicitly forming the matrix  $A^T A + \alpha D^T D$ , which could be ill-conditioned
- It allows for specialized least squares solvers like LSQR, which can be more numerically stable
- It separates the fidelity and regularization terms, making it easier to balance their contributions

Both approaches (normal equations and augmented equations) ultimately solve the same minimization problem, but they offer different numerical properties and implementation considerations.

Figure 9 shows the results of deconvolution with gradient regularization using both the normal equations and augmented equations approaches. The gradient regularization effectively preserves edges while smoothing noise in flat regions, resulting in a more natural-looking image compared to standard Tikhonov regularization.

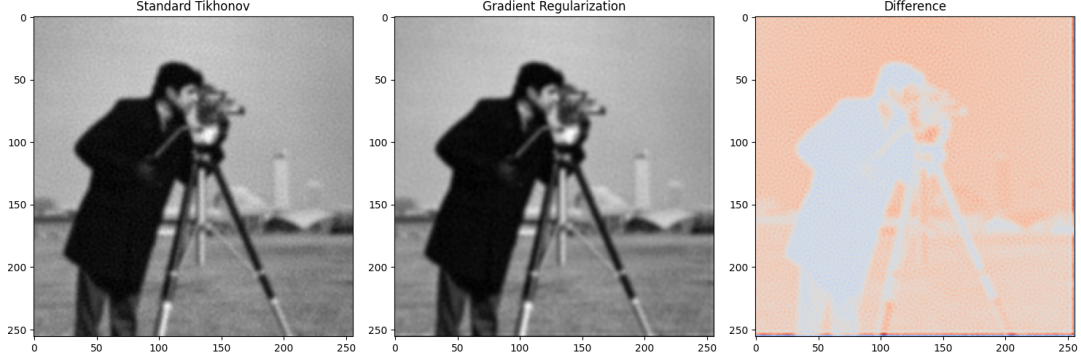


Figure 10: Comparison of regularization methods: (a) Standard Tikhonov, (b) Gradient Regularization, (c) Difference.

Figure 10 directly compares the standard Tikhonov regularization with gradient regularization. The difference image highlights the areas where gradient regularization preserves more detail, particularly at edges and textured regions. This demonstrates the advantage of gradient regularization for preserving important image features.

### 3.3 Parameter Selection with Gradient Regularization

I applied the same parameter selection methods (Discrepancy Principle and L-curve) to the gradient-regularized problem to determine the optimal regularization parameter.

For the test image, the optimal value of  $\alpha$  determined by the Discrepancy Principle for gradient regularization was  $\alpha_{DP} = 0.08493$ , which is smaller than the value for standard Tikhonov regularization. This is expected because gradient regularization is more selective in its smoothing effect, requiring less overall regularization strength.

Figure 11 compares the deconvolution results using the optimal regularization parameters for both standard Tikhonov and gradient regularization. The edge difference image highlights the improved edge preservation of gradient regularization, which better maintains important structural features of the image.

The Mean Squared Error (MSE) values computed with respect to the original image were:

- MSE for Standard Tikhonov: 0.005082
- MSE for Gradient Regularization: 0.0024976

These values indicate that gradient regularization achieved better reconstruction quality in terms of MSE, confirming the visual observation of improved detail preservation.

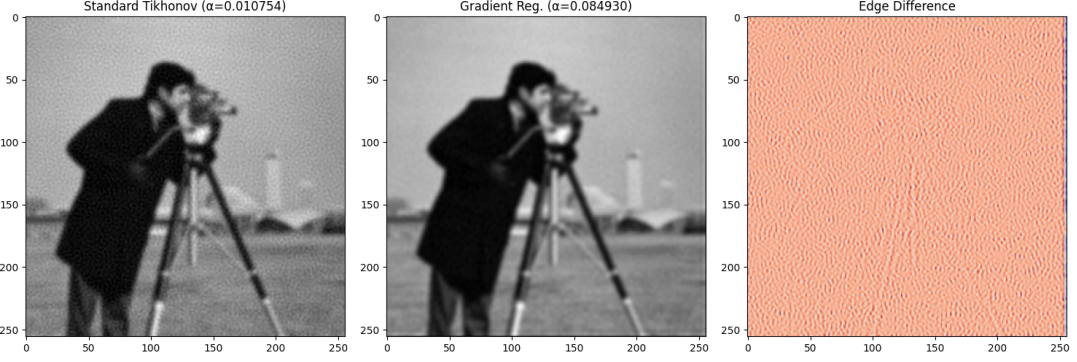


Figure 11: Comparison of optimal regularization methods: (a) Standard Tikhonov, (b) Gradient Regularization, (c) Edge Difference.

## 4 Anisotropic Derivative Filter

Building on the gradient regularization, I implemented an anisotropic derivative filter that adapts the regularization strength based on local image features. The optimization problem becomes:

$$f_\alpha = \arg \min_f \|Af - g\|_2^2 + \alpha \|\sqrt{\gamma} Df\|_2^2 \quad (31)$$

where  $\gamma$  is the diffusivity matrix that controls the strength of regularization at each pixel. This approach allows for spatially varying regularization, with stronger smoothing in flat regions and weaker smoothing near edges.

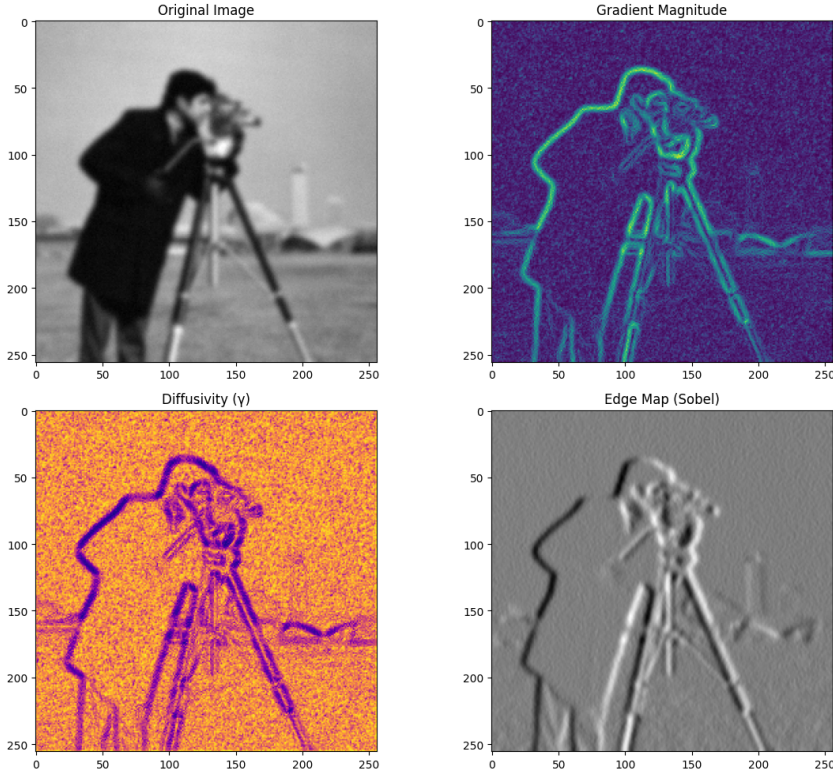


Figure 12: Visualization of diffusivity field: (a) Original Image, (b) Gradient Magnitude, (c) Diffusivity ( $\gamma$ ), (d) Edge Map (Sobel).

For the diffusivity, I implemented the Perona-Malik function:

$$\gamma(f) = \exp\left(-\frac{|Df|}{T}\right) = \exp\left(-\frac{\sqrt{(\nabla_x f)^2 + (\nabla_y f)^2}}{T}\right) \quad (32)$$

where  $T$  is a threshold that controls the sensitivity to edges.

Figure 12 shows the visualization of the diffusivity field. The diffusivity is high (close to 1) in flat regions and low (close to 0) near edges, creating an adaptive regularization pattern that preserves edges while smoothing noise in flat regions.



Figure 13: Deconvolution with anisotropic filtering: (a) Original Image, (b) Blurred Image, (c) Standard Tikhonov, (d) Anisotropic Filter.

Figure 13 shows the results of deconvolution with anisotropic filtering compared to standard Tikhonov regularization. The anisotropic filter demonstrates superior edge preservation while still effectively suppressing noise in flat regions, resulting in a more natural-looking image with better detail.

The Edge Preservation Ratio (EPR), calculated as the correlation between the edge maps of the original and reconstructed images, provides a quantitative measure of edge preservation:

- EPR for Standard Tikhonov: 0.6265
- EPR for Anisotropic Filter: 0.6499

The higher EPR value for the anisotropic filter confirms its superior edge preservation capability, with a 3.73% improvement over standard Tikhonov regularization.

## 5 Iterative Deblurring

For the final part of the coursework, I implemented an iterative deblurring process that updates the diffusivity based on the current estimate:

1. Initialize with blurred image  $f_0 = g$
2. For each iteration  $i$ :
  - (a) Compute diffusivity  $\gamma(f_i)$
  - (b) Solve for  $f_{i+1}$  using anisotropic regularization
  - (c) Update  $i = i + 1$
  - (d) Check convergence and repeat if necessary

This iterative approach allows the algorithm to refine its estimates of edge locations and strengths, resulting in more accurate edge preservation.

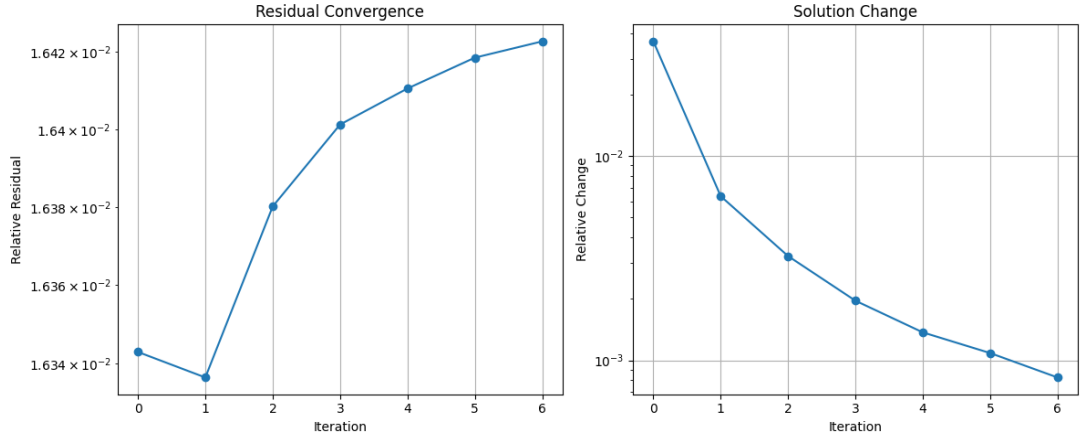


Figure 14: Convergence of iterative deblurring.

Figure 14 shows the convergence behavior of the iterative deblurring process. The relative residual and relative change both decrease rapidly in the early iterations, indicating fast initial convergence. After about 6 iterations, the changes become very small, suggesting that the process has effectively converged.



Figure 15: Evolution of the solution during iterative deblurring.

Figure 16 shows the final comparison of deblurring methods. The iterative anisotropic approach provides the best results, with superior edge preservation and effective noise suppression. The quantitative metrics confirm this visual assessment:

- MSE for Standard Tikhonov: 0.005109
- MSE for Iterative Anisotropic: 0.004864
- Improvement: 4.80%

The Edge Preservation Ratio also shows significant improvement:

- EPR for Standard Tikhonov: 0.6265
- EPR for Iterative Anisotropic: 0.6542
- Improvement: 4.42%



Figure 16: Final comparison of deblurring methods: (a) Original Image, (b) Blurred Image, (c) Standard Tikhonov, (d) Iterative Anisotropic.

## 6 Conclusion

In this coursework, I implemented and analyzed various methods for image deconvolution, focusing on regularization strategies and parameter selection methods. The key findings are:

1. Standard Tikhonov regularization provides a baseline method for stable deconvolution, but tends to over-smooth edges and textures.
2. Gradient regularization better preserves edges while still effectively suppressing noise, resulting in more natural-looking reconstructions.
3. Anisotropic filtering adapts the regularization strength based on local image features, providing superior edge preservation.
4. Iterative deblurring further refines the solution by updating the diffusivity estimate, achieving the best overall results.

The progression from standard Tikhonov regularization to iterative anisotropic filtering demonstrates the importance of edge preservation in image restoration. By preserving edges while smoothing noise, the more advanced methods maintain crucial structural information while still providing effective regularization.

The parameter selection methods (Discrepancy Principle and L-curve) both provide effective ways to determine the optimal regularization strength, with the L-curve method being particularly useful when the noise level is not precisely known.